Sea Surface Temperature Variability along the Path of the Antarctic Circumpolar Current

ARIANE VERDY, JOHN MARSHALL, AND ARNAUD CZAJA

Department of Earth, Atmospheric and Planetary Sciences, and MIT–WHOI Joint Program in Oceanography, Massachusetts Institute of Technology, Cambridge, Massachusetts

(Manuscript received 23 February 2005, in final form 16 November 2005)

ABSTRACT

The spatial and temporal distributions of sea surface temperature (SST) anomalies in the Antarctic Circumpolar Current (ACC) are investigated, using monthly data from the NCEP–NCAR reanalysis for the period 1980–2004. Patterns of atmospheric forcing are identified in observations of sea level pressure and air–sea heat fluxes. It is found that a significant fraction of SST variability in the ACC can be understood as a linear response to surface forcing by the Southern Annular Mode (SAM) and remote forcing by ENSO. The physical mechanisms rely on the interplay between atmospheric variability and mean advection by the ACC. SAM and ENSO drive a low-level anomalous circulation pattern localized over the South Pacific Ocean, inducing surface heat fluxes and Ekman heat advection anomalies. A simple model of SST propagating in the ACC, forced with heat fluxes estimated from the reanalysis, suggests that surface heat fluxes and Ekman heat advection are equally important in driving the observed SST variability. Further diagnostics indicate that SST anomalies, generated mainly upstream of Drake Passage, are subsequently advected by the ACC and damped after a couple of years. It is suggested that SST variability along the path of the ACC is largely a passive response of the oceanic mixed layer to atmospheric forcing.

1. Introduction

In the Southern Ocean, sea surface temperature (SST) anomalies are observed to propagate eastward; it has been suggested that the signal encircles the globe in 8–10 yr (White and Peterson 1996). This low-frequency variability arises from mechanical and thermodynamic forcing at the air–sea interface. Mechanisms controlling the spatial and temporal scales of SST variability in the Southern Ocean are not well understood, nor is the extent to which coupled ocean–atmosphere interactions play a role.

Remote forcing by El Niño–Southern Oscillation (ENSO) has been proposed as a trigger of SST variability (Cai and Baines 2001; White and Peterson 1996), through teleconnections with the Tropics. ENSO has also been linked to sea ice extent variability around Antarctica (Yuan and Martinson 2000). In contrast, based on the result of their numerical model, Hall and Visbeck (2002) have argued that much of the variability in the Southern Ocean, including SST, is forced locally by the Southern Annular Mode (SAM), a dominant source of atmospheric variability in the Southern Hemisphere.

The role of ocean dynamics in the generation and maintenance of SST anomalies has also been examined (see, e.g., Haarsma et al. 2000). The presence of the Antarctic Circumpolar Current (ACC), a strong eastward flow in a zonally periodic domain, can lead to interesting dynamics. Away from the frontal jets, the speed of the flow in the ACC is similar to the propagation speed of SST anomalies, and it is tempting to believe that the ACC is involved in carrying the anomalies. However, whether the signal will propagate significant distances depends on the rates of advection and damping. Decay of SST anomalies through interaction with the atmosphere typically occurs over a period of a few months (Frankignoul 1985). This implies that visual propagation of the signal would not be possible without a mechanism that maintains the anomalies in the face of damping.

Two explanations have been put forward for the observed persistence of SST variability. The first is based

Corresponding author address: Ariane Verdy, Massachusetts Institute of Technology, Rm. 54-1419, 77 Massachusetts Ave., Cambridge, MA 02139.
E-mail: averdy@ocean.mit.edu

on the interplay between stochastic atmospheric forcing and ocean advection (Haarsma et al. 2000; Weisse et al. 1999), while the second relies on the growth of coupled modes of the ocean–atmosphere system (Goodman and Marshall 1999, 2003; Qiu and Jin 1997; Talley 1999; White et al. 1998) that act against damping processes, thus increasing the longevity of SST anomalies. The main difference between the two mechanisms lies in the role of the ocean, whether passively responding to atmospheric forcing or actively involved in the ocean–atmosphere coupling.

The hypothesis of an active role for the ocean was motivated by the observation of a phase-locked propagation of sea level pressure (SLP) and SST anomalies (White and Peterson 1996). The phenomenon was dubbed the Antarctic Circumpolar Wave (ACW) by White and Peterson (1996) due to the apparent periodicity of the signal. SLP anomalies are observed to lag SST anomalies by 1/4 wavelength. This configuration suggests that atmospheric circulation is dynamically affected by oceanic feedbacks, in such a way that the anomalies grow in time. Following the idea of midlatitude ocean–atmosphere coupling of Latif and Barnett (1994), White et al. (1998) proposed a mechanism in which SST anomalies are amplified by meridional advection of warm (cold) air resulting from vortex stretching over warm (cold) water. In the two-layer ocean model of Qiu and Jin (1997), the equivalent barotropic response of the atmosphere induces a wind stress curl downstream of SST anomalies, which are then reinforced though Ekman pumping in the ocean. Such scenarios involving ocean feedbacks are controversial, as there is little observational evidence for extratropical coupled modes. Cases in which the oceanic feedbacks have a considerable impact on the local climate are more commonly found in the Tropics (Kushnir et al. 2002).

Mechanisms that do not require ocean–atmosphere coupling have also been put forward to interpret interannual SST variability. The analytical model of Saravanan and McWilliams (1998) shows that in the presence of a mean oceanic flow, it is possible to obtain decadal variability and propagation in the SST signal as a passive response to atmospheric forcing. The theory is based on the idea of a stochastic climate model proposed by Hasselmann (1976): low-frequency variability arises in the ocean from a slow response to random atmospheric forcing. If an advective ocean interacts with a spatially fixed forcing that is stochastic in time, a preferred time scale will be excited in the ocean, determined by the ratio of the length scale of the forcing and the speed of the mean flow. Saravanan and McWilliams (1998) explained decadal variability in the North Atlantic as a result of this "advective resonance" mechanism, where SST anomalies advected by the Gulf Stream interact with a dipole pattern of atmospheric forcing, identified with the North Atlantic Oscillation (NAO). In the Southern Ocean, one can think of a similar set of circumstances, in which advection by the ACC combined with standing patterns of atmospheric forcing associated with, for example, ENSO and SAM, lead to decadal signals.

The advective resonance mechanism can explain the ACW-like variability in the models of Weisse et al. (1999) and Haarsma et al. (2000). In these numerical experiments, it is found that SST variability is excited by the dominant modes of variability in the atmosphere, which appear to have a wavenumber-2 or wavenumber-3 spatial pattern. The authors do not specifically identify the source of atmospheric variability behind these forcing patterns. Stochasticity of the forcing is a key element of the mechanism: there exists a frequency for which, by the time it takes an SST anomaly to travel from one pole of the forcing to the next, the forcing has reversed polarity, so that the anomaly created initially gets amplified. This process competes against damping of the anomalies, and is responsible for their apparently long persistence. It results in a visual propagation of the SST signal, in the direction of ocean advection. Advective time scales become amplified in the SST spectrum; the spectrum is easily found analytically for a sinusoidal spatial pattern (Saravanan and McWilliams 1998); Scott (2003) solved it for a periodic domain.

The motivation for the present study is to understand the physical mechanisms leading to observed interannual SST variability in the Southern Ocean. Our goal is to assess the role of ocean dynamics and atmospheric forcing. In particular, we focus on the role of ENSO and SAM, the former because of its well-documented role in oceanic variability, especially in the tropical Pacific Ocean but also in the tropical Atlantic Ocean (Czaja et al. 2002) and North Pacific (Alexander et al. 2002), and the latter because it is dynamically similar to the NAO, which also is known to drive variability in the ocean (Marshall et al. 2001). We wish to put forward the view that SST variability along the path of the ACC can simply be understood as a passive response of the ocean mixed layer to SAM and ENSO forcing. Mechanisms involve primarily mean oceanic advection and anomalous surface heating and/or cooling through surface heat flux (F_s) and Ekman advection (F_{ek}).

The layout of the paper is as follows: observations of the variability in the ACC are described in section 2. In section 3, a simple model of SST propagating in the mixed layer is forced with observed heat fluxes (F_s +

FIG. 1. Two geostrophic streamlines encircling the globe, delimiting the region of the ACC, plotted over the data grid points (from NCEP–NCAR reanalysis); for clarity only one-half of the points are shown in the zonal direction. Shaded areas represent landmasses and sea ice.

F_{ek}), in order to identify which components of the heat fluxes are important in explaining the observed SST variability. The relevance of ENSO and SAM in driving those heat fluxes is presented in section 4. In section 5, the physical mechanism is related to the resonant advection mechanism of Saravanan and McWilliams (1998), and the spectral response of the ocean to ENSO and SAM forcing is examined. Ocean–atmosphere coupling is discussed in section 6, and the main results are summarized in section 7.

2. Observed variability in the ACC

a. Methodology

We use the dataset from the National Centers for Environmental Prediction–National Center for Atmospheric Research (NCEP–NCAR) reanalysis (Kalnay et al. 1996) over the period 1980–2004. This period is chosen because it incorporates satellite-based SST estimates: from 1982 onward, the reanalysis employs Reynolds SST (analyzed data from the Advanced Very High Resolution Radiometer, AVHRR). Prior to the 1980s, SST observations were limited to ship and buoy measurements. Other fields used in this study, such as heat fluxes, are not directly constrained by observations and thus are subject to larger inaccuracies; for the more recent period, however, the modeled variables show similar statistics to that of the European Centre for Medium-Range Weather Forecasts (ECMWF) reanalysis (Sterl 2004), suggesting reasonable reliability.

Surface data are provided on a grid with a resolution of approximately 2° × 2°; in this study, we consider monthly averages. All time series are linearly detrended, but otherwise not filtered. The variability is computed by removing the mean seasonal cycle, calculated at every grid point. Departures from the seasonal cycle are defined as "anomalies."

The variability is analyzed along the path of the ACC. For this purpose, we estimate the position of the current using sea surface height data from the Ocean Topography Experiment (TOPEX)/Poseidon altimeter. Following Karsten and Marshall (2002), the 4-yr-averaged dynamic sea surface height is compared with a reference geoid to evaluate the geostrophic streamfunction (Ψ):

$$\Psi = \frac{gh}{f}, \tag{1}$$

where f is the Coriolis parameter, g is the gravitational constant, and h is the sea surface height. The geostrophic flow is given by the gradient of Ψ:

$$(u_g, v_g) = \mathbf{z} \times \nabla\Psi, \tag{2}$$

where $\mathbf{z}$ is a unit vector in the vertical direction.

The mean path of the ACC is defined here as the region bounded by the two circumpolar streamlines that flow around the globe without intercepting land (Fig. 1). Observations are averaged over the width of the current. This procedure is justified by the fact that the dominant structures of anomalous SST and surface heat fluxes, obtained from empirical orthogonal function (EOF) analysis, exhibit little variations across the ACC (not shown). Data falling on sea ice are excluded. Landmasses and sea ice are shaded in Fig. 1.

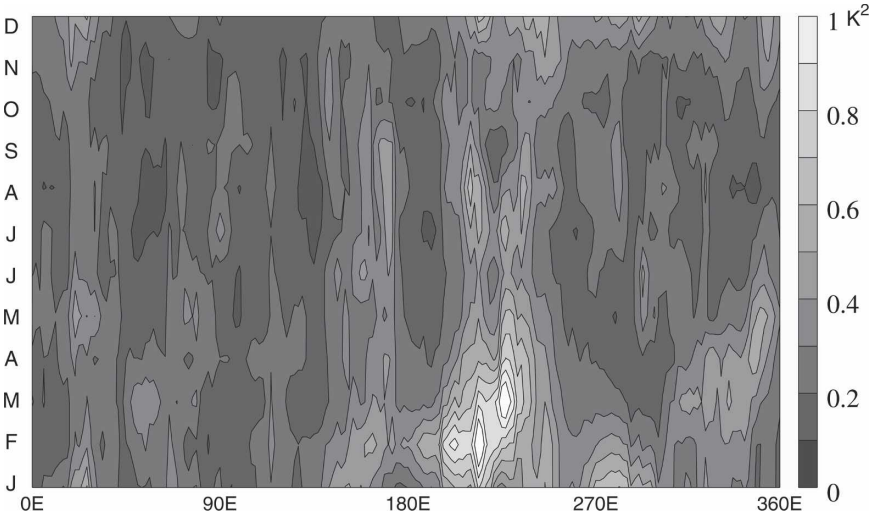

FIG. 2. Variance of SST anomalies along the ACC (x axis is longitude), as a function of calendar month. The variability is greatest in the Pacific sector (200°–300°E); it is enhanced during the austral summer when the mixed layer is shallowest.

b. Along-stream variability of SST

First we examine the distribution of SST anomalies in time and space. In Fig. 2, the variance of surface temperature anomalies along the path of the current is presented as a function of calendar month. Monthly SST anomalies have typical magnitudes of 1 K; the interannual signal is thus not negligible relative to the seasonal cycle, which has a total amplitude of approximately 3 K (not shown). Most of the variability occurs in the central Pacific, between 200° and 300°E. At those latitudes the current flows closest to sea ice (Fig. 1). It also coincides with the end of the storm track (Nakamura and Shimpo 2004), associated with enhanced wind variability. For these two reasons, the heat fluxes are expected to be more variable in this region, driving anomalous SST.

Seasonal variations are evident in Fig. 2; the variance is strongest during the austral summer months (January–March). This time dependence is thought to result from variations in mixed layer depth: unlike in the Northern Hemisphere, atmospheric forcing in the Southern Hemisphere exhibits little seasonal variation; the amplitude of anomalous heat fluxes at the sea surface being constant throughout the year, the resulting SST anomalies are less important when the mixed layer is deep, which happens in the winter when mode waters are forming (Levitus and Boyer 1994).

The dominance of SST variability in the Pacific was also observed by Cai and Baines (2001), who relate it to the location of the Pacific–South America pattern, a surface pressure anomaly. Yuan and Martinson (2000) observe that sea ice variability is strongest in the Pacific.

c. Along-stream covariability of SST and SLP

The SST variability is now related to sea level pressure (SLP) fluctuations through a maximum covariance analysis (mca) of streamline-averaged anomalies. This technique, also called singular value decomposition, is used to identify the orthogonal modes of variability in two covarying fields (Bretherton et al. 1992). It is performed here on monthly data; for the 24-yr period considered, the analyzed time series have 288 data points.

Figure 3 shows the patterns and their associated time series for the two leading modes of covariability, accounting for 63% and 21% of the squared covariance, respectively. The first mode accounts for 20% of the SST variance, and 24% of the SLP variance (as a reference, the first EOFs of streamline-averaged SST and SLP explain 22% and 27% of their respective variances). The time series associated with the first mca mode will be subsequently referred to as SST-mca and SLP-mca. The second mode, which has weaker amplitude, accounts for 11% and 21% of the SST and SLP variances, respectively. These spatial patterns are essentially localized in the Pacific basin, both for temperature and pressure anomalies.

For both modes, the SLP maximum is slightly to the east of the SST maximum; in the Pacific they are separated by roughly 45° in longitude. A simple explanation is that the advection of air around the high pressure center is reinforced by advection of air around the low pressure anomaly at 200°E; both drive ocean–atmosphere exchanges of heat around 250°E, which is the location of the SST-mca maximum. The spatial configuration supports the idea that heat fluxes induced by

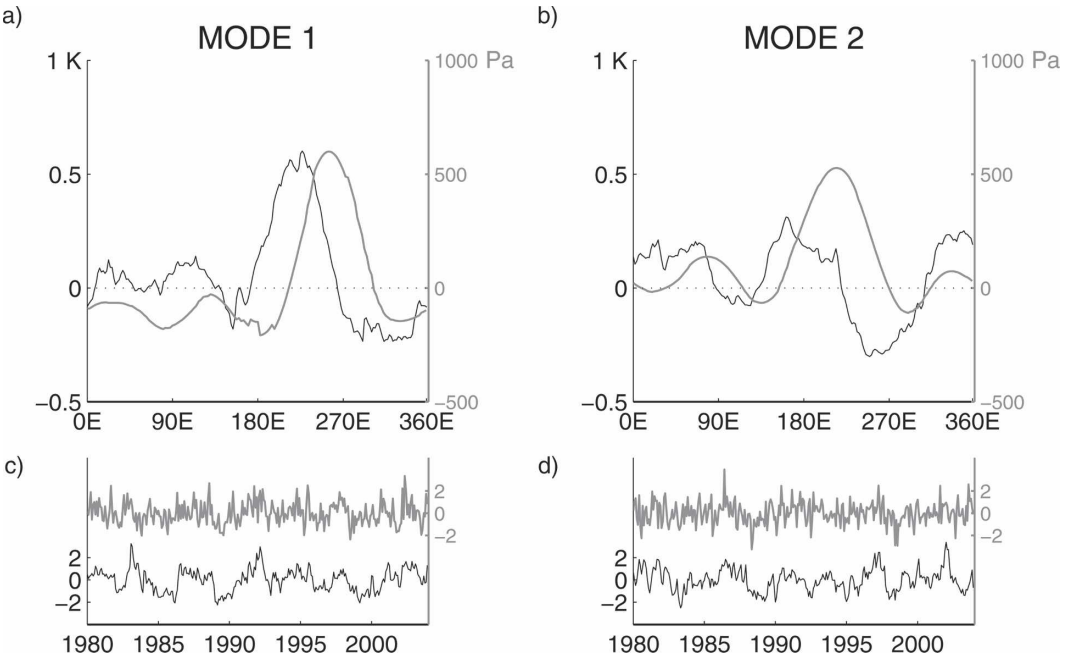

FIG. 3. First and second modes of variability of SST (black) and SLP (gray) showing the maximum covariance along the ACC. The spatial patterns for (a) mode 1 and (b) mode 2. Mode 2 is upstream of mode 1 and has weaker amplitude. The amplitude shown corresponds to a typical change in SST (K) or SLP (Pa) for 1 std dev of the associated time series. (c), (d) The normalized time series associated with the spatial patterns.

anomalous low-level atmospheric circulation are involved in the generation of SST anomalies. Similar analysis with covarying SST and meridional winds shows that the position of maximum winds does indeed coincide with the SST maximum (not shown).

We also find that the covariance between SST-mca and SLP-mca is a maximum when the pressure signal leads by 1 month. This time lag is consistent with the scenario of a passive response of the ocean to atmospheric forcing, the ocean taking a few weeks to adjust to the change in heat fluxes. This result suggests that SST is driven by the SLP mode, and not vice versa. Based on these observations, we claim that SST variability in the ACC is forced by a low-level atmospheric pattern localized in the Pacific.

d. Propagating modes of SST variability

From the mca, we find that the SLP signal is essentially standing; its autocorrelation has an *e*-folding time scale of only 1 month. For this reason it is hard to obtain evidence for the propagation of SLP anomalies, and indeed our analysis revealed no significant indication of propagation. On the other hand, we find that SST modes 1 and 2 are not independent, but correspond to a single propagating mode. The second mode leads the first by approximately 1 yr (correlation not shown here). The propagation of the SST anomalies is highlighted by performing a lagged correlation of the SST-mca mode with the time series of observed SST at every longitude, along the path of the ACC (Fig. 4). In the figure, shaded regions indicate where correlations are significant at the 95% level; we take 3 months as a null hypothesis for midlatitude SST decorrelation time, thus assuming $N/3$ degrees of freedom for a time series containing N data points.

At zero lag, following the horizontal dashed line, the pattern in Fig. 3 is retrieved: the amplitude of the signal is greatest in the central Pacific. As the lag increases, the peak correlation moves to the right, indicating that the pattern of anomalous temperature has moved eastward. From the slope of the correlation bands in Fig. 4 we infer the propagation speed to be 8 cm s^{-1}. This value coincides with the mean geostrophic velocity of the ACC, estimated from the geostrophic streamfunction defined in (2). The meridional gradient of Ψ calculated from the two circumpolar streamlines shown in Fig. 1 gives the geostrophic velocity averaged across the current; the average of this velocity along the current is 8 cm s^{-1}. This suggests that the SST anomalies are passively advected by the current.

Significant correlations appear to be centered around the Pacific basin and limited to ± 2 yr lag. The fact that higher correlations are found downstream (positive lag) than upstream of the Pacific suggests that anomalies

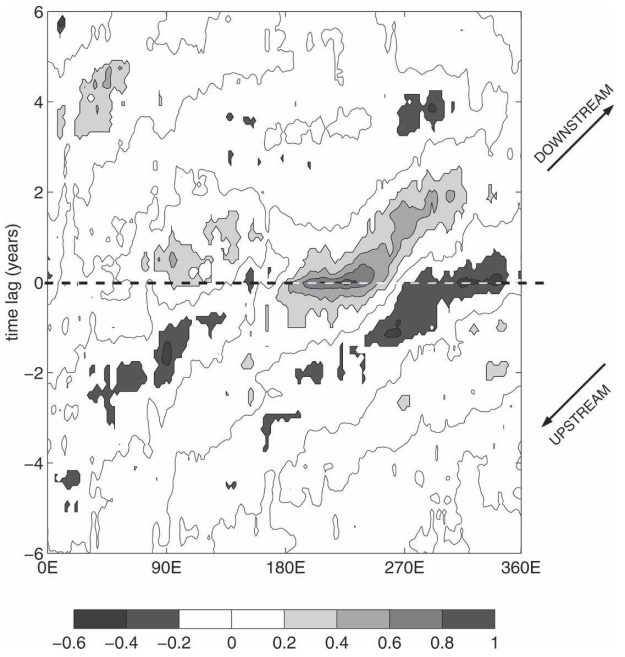

FIG. 4. Lagged correlation of observed SST with the first SST-mca mode (from Fig. 3). At zero lag, following the horizontal dashed line, the pattern in Fig. 3a is retrieved. Lighter shades of gray indicate positive correlations and darker shades show negative correlations; only values that are significant at the 95% level are shown. The location of the maximum correlation (~210°E at zero lag) is displaced to the right as lag increases, indicating eastward propagation of the signal. The speed of propagation is estimated from the figure to be 8 cm s^{-1}, which coincides with the mean advection velocity of the ACC. If they persisted, anomalies propagating at that speed would encircle the globe in approximately 10 yr.

originate from that region and are then advected away. In addition, a superposition of wavenumbers 1 and 2 appears to dominate the spatial structure. In the next section, we show that these characteristics can be understood as a response of the mixed layer to mean oceanic advection and anomalies in surface heat flux and Ekman advection. In sections 4 and 5 we will argue that the wavenumbers 1 and 2 reflect SAM and ENSO forcing.

3. A diagnostic model of the SST anomaly

To study the extent to which the observed SST variability can be explained by observed heat fluxes, we employ a one-dimensional model of SST propagating in the ACC. It is forced by observed heat fluxes.

a. Heat flux variability

Turbulent surface heat fluxes occur via the exchange of latent and sensible heat at the air–sea interface. The sensible heat flux and latent heat flux are obtained from the reanalysis, and summed. As a preliminary diagnostic, we calculated the surface heat fluxes from the linearized bulk formulas, and found the calculated values to be very similar to those of the reanalysis. The two components of the linearized bulk formulas contributing to heat flux variability have similar magnitude; one is due to anomalous wind and the other is due to anomalous temperature and moisture at the sea surface. Together the two components add up to surface anomalous heat fluxes with a standard deviation of 12–28 W m^{-2}, depending on the position along the current.

In addition, we consider heat fluxes resulting from anomalous Ekman advection in the upper ocean, acting on mean temperature gradients (especially in the meridional direction). We estimate Ekman fluxes from wind stress anomalies from the reanalysis:

$$F'_{\mathrm{ek}} = \rho c_p(\mathbf{u}'_{\mathrm{ek}} \cdot \nabla \overline{T}), \tag{3}$$

where $\mathbf{u}'_{\mathrm{ek}} = -(1/\rho f)(\mathbf{z} \times \boldsymbol{\tau}')$ is the anomalous Ekman transport in the ocean, $\boldsymbol{\tau}'$ is the wind stress anomaly and $\nabla\overline{T}$ is the seasonally varying SST gradient, f is the Coriolis parameter, $\mathbf{z}$ is a unit vector in the vertical direction, and ρ and c_p are the density and heat capacity of seawater, respectively.

b. Description of the model

The model is set up in a similar fashion as the stochastic model with ocean advection of Saravanan and McWilliams (1998), but in our case the random forcing is replaced by the observed heat fluxes described above. Here we consider oceanic advection along the x axis, which we choose to be parallel to the path of the ACC defined in section 2. Heat flux data are averaged meridionally over the width of the current.

The temperature equation in the mixed layer, linearized around the mean seasonal cycle, is

$$\frac{\partial}{\partial t} T' + \overline{u}\frac{\partial}{\partial x} T' = \frac{1}{\rho c_p h}[-\alpha T' + (F'_{\mathrm{ek}} + F'_{\mathrm{s}})]. \tag{4}$$

For the advective velocity, we take the mean geostrophic velocity of the ACC, $\overline{u} = 8$ cm s^{-1}. This value was determined as the temporal and spatial average of the along-ACC velocity calculated from TOPEX/Poseidon data (section 2a). The depth of the mixed layer, h, is assumed constant with a value of 100 m. From the Levitus climatology, we know that h is spatially inhomogeneous and that it varies seasonally from about 50 m in the austral summer to more than 500 m in the winter in convective locations; however, we found that taking a constant value does not qualitatively affect the result of the simulation. Similarly, choosing a different value for h (still constant) affects

the magnitude but not the patterns of simulated SST anomalies. By considering uniform velocity and uniform depth, we ensure that the transport is constant along the current, assuming that the bounding streamlines separation does not vary.

The damping parameter α represents the terms that are not explicitly included in (4): vertical entrainment and horizontal diffusivity. We choose a value of $\alpha = 20$ W m^{-2} K^{-1} for this tunable parameter, which corresponds to a damping time scale of roughly 8 months for a mixed layer depth of 100 m. This value gives the most realistic persistence of SST anomalies. The temperature equation is integrated numerically; it is discretized using a forward in time, upwind in space scheme. This scheme leads to numerical damping, but we find it to be negligible relative to the time scale of damping to the atmosphere. Initially, the anomalous SST field is set to observed values for January 1980.

c. Simulated SST variability

The simulated SST is presented in Fig. 5 as a function of longitude and time. It was obtained by introducing the observed heat flux and Ekman advection of heat into (4). The high frequencies of the forcing are filtered out by the model; this is explained by the slow oceanic response (causing the reddening of the SST spectra in Hasselmann's theory). For comparison, the observed SST field is also presented in Fig. 5 as a function of longitude and time. A visual examination of the two diagrams reveals that the model captures the propagation and timing of the observed basin-scale SST. Eastward propagation in the modeled field occurs at the prescribed velocity (8 cm s^{-1}). The agreement between simulated and observed fields is particularly good in the Pacific and western Atlantic.

A quantitative comparison of the simulation with the observations is obtained by cross-correlating their respective EOFs. The first mode of variability of the observed SST is strongly peaked around 230°E (in the Pacific) and accounts for 22% of the variance. For the simulated SST, the first EOF, accounting for 32% of the variance, has a different spatial pattern; the peak centered in the Pacific is retrieved in the second EOF, which accounts for 27% of the variance. The correlation coefficient between EOF1 of the observations and EOF2 of the simulation is 0.48.

Differences between the two fields can be explained by the simplicity of the model, which does not represent uncertainties in the forcing, eddy turbulence, vertical entrainment, and other ocean dynamics. These processes are responsible for spatial and temporal small-scale variability, not captured by the model.

Figure 6 shows that both the simulated and observed fields exhibit more variability in the Pacific basin. Since the model's mixed layer depth is constant in space, this enhanced variability must arise from spatial inhomogeneity of the surface forcing. Inspection of the heat fluxes does indeed reveal that their variance is greater in the Pacific than in other basins, consistent with the analysis of section 2c. The amplitude of the simulated variance is sensitive to the choice of α; stronger damping induces weaker variability. The value $\alpha = 20$ W m^{-2} K^{-1} leads to simulated SST variance that is similar to the observations.

The relative importance of the surface heat fluxes versus Ekman advection can be assessed by performing simulations with each component separately. SST driven from Ekman fluxes alone, as well as SST driven from surface fluxes alone, have more variability in the Pacific (Fig. 6). In both cases, SST variance is considerably less than when the total heat flux field is used. This indicates that Ekman and surface fluxes reinforce rather than cancel one another. The magnitude and variance of simulated SST anomalies is similar in both cases, suggesting that Ekman and turbulent fluxes are each responsible for approximately 50% of the SST variability.

4. Mechanisms of external forcing

a. SAM and ENSO

Since we have demonstrated in section 3 that $F_s + F_{ek}$ is the main driver of SST variability along the ACC, we now investigate what physical mechanisms drive the observed heat fluxes. From the maximum covariance analysis presented in section 2, a coupled system seems unlikely, since the SLP variability tends to lead in time the SST variability. The other possible scenario is one in which the ocean reacts passively to the forcing. In this case one can ask: what are the primary sources of atmospheric variability?

We examine two sources of atmospheric forcing: ENSO and SAM. ENSO is a coupled ocean–atmosphere phenomenon originating in the Tropics. It is thought to reach the ACC via atmospheric teleconnections: possible mechanisms include propagation of the signal by atmospheric Rossby waves (Karoly 1989), and changes in the Ferrel cell (Liu et al. 2002). We use Niño-3 as an index for ENSO-related variability (Cane et al. 1986); it is calculated from the SST averaged between 5°S and 5°N, from 150° to 90°W. Most of its energy is in the 3–7-yr-period band (Wunsch 1999).

SAM is an important source of monthly and interannual variability in the atmosphere, also referred to as the Antarctic Oscillation (AAO). In its positive phase it

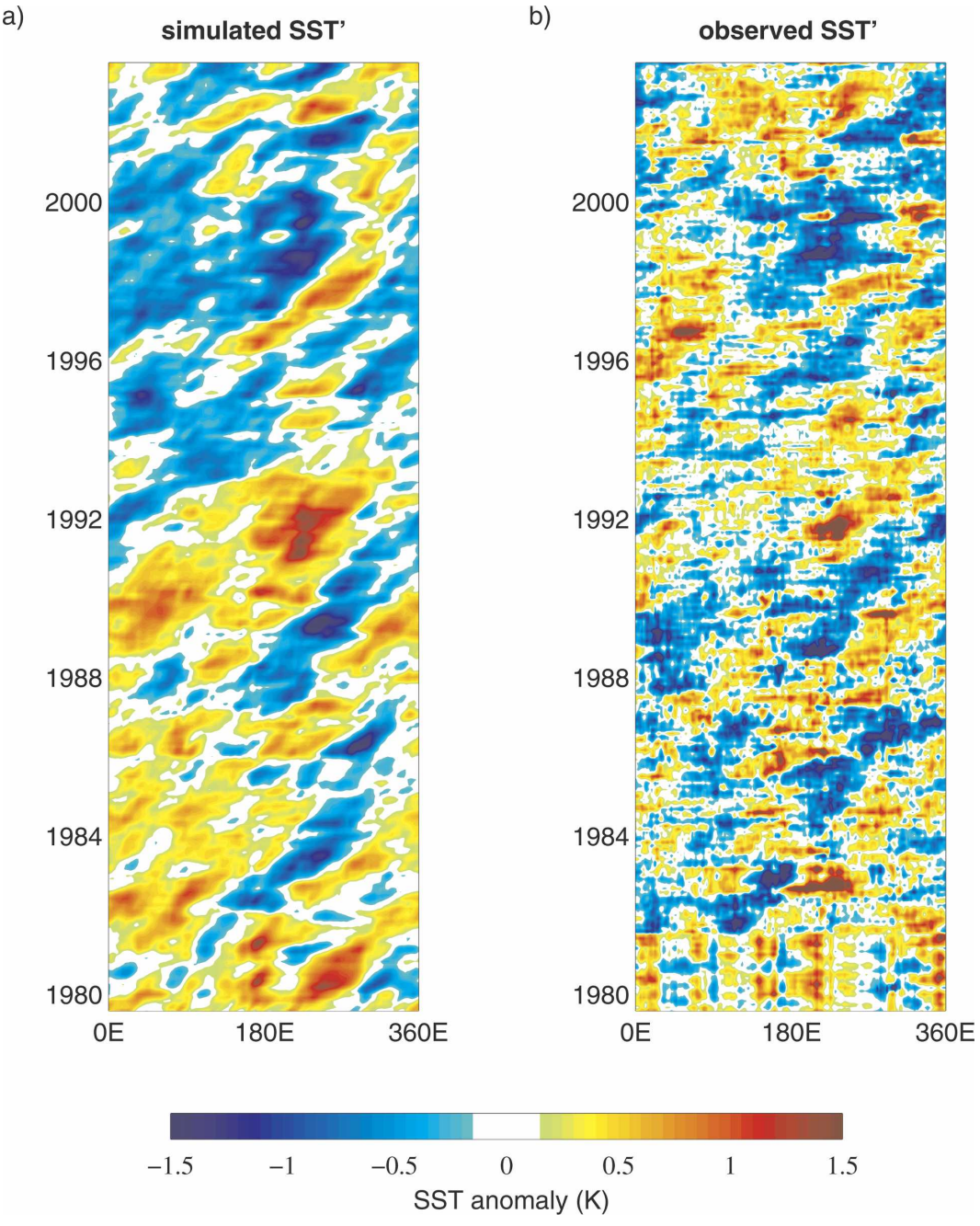

FIG. 5. Time–longitude diagrams of (a) the SST simulated from the heat fluxes, estimated from the reanalysis and introduced in (4), and (b) observed SST from the reanalysis. The simulated field captures the propagation and timing of the observations.

is characterized by a contraction of the polar vortex (Thompson and Wallace 2000), which is expressed at the sea surface by an enhancement of the westerlies in the region of the ACC. A measure of the strength of SAM is given by the "SAM index," calculated from the principal component of the first mode of variability of the 850-hPa field between 20° and 90°S (Thompson and Wallace 2000). On time scales of a month or longer, it has a white spectrum.

The two indices are found to be strongly correlated with the SST signal. The SAM and Niño-3 indices are plotted in Fig. 7, along with the time series of SST-mca. One observes a close correspondence between all time series, with the lagged cross correlations peaking when

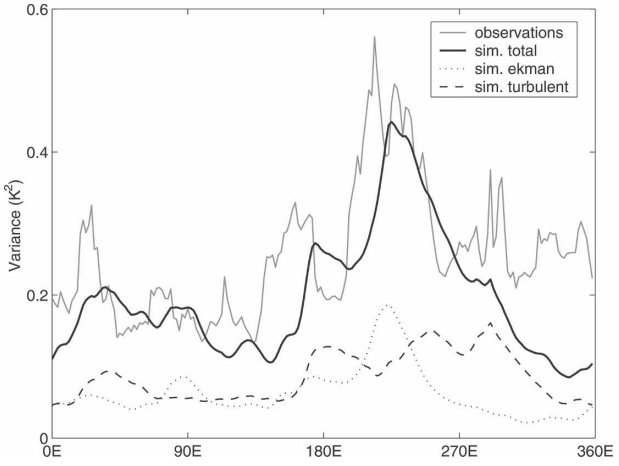

FIG. 6. Variance of SST as a function of longitude (along the path of the SST): observations (gray line), simulated from Ekman heat fluxes (dotted line), simulated from surface heat fluxes (dashed line), and simulated from Ekman plus surface heat fluxes (black solid line).

SAM and ENSO lead in time; this is consistent with an atmospheric driving of SST variability. It is found that the correlation with Niño-3 has a coefficient of 0.53, when the temperature lags by 1 month. The correlation with SAM has a coefficient of −0.38, when the temperature lags by 1 month; the correlation is −0.47 when seasonal averages are considered. Together ENSO and SAM explain approximately 45% of the leading mode of SST covarying with the atmosphere (the fraction of variance explained is given by the square of the correlation coefficient). In such estimates, we have assumed that the annular mode is independent of ENSO. This hypothesis seems reasonable as they have very different dynamics, and we were unable to show any dependence of one index upon the other.

The SLP-mca mode is also found to be associated with SAM and ENSO. The correlation coefficient between SLP-mca and ENSO is 0.33, and with SAM it is −0.58 (0.43 and −0.65 for seasonal averages).

ENSO and SAM are both found to affect the low-level atmospheric circulation in the South Pacific. The patterns can be seen in Fig. 8, showing the correlations of monthly SLP anomalies (from the reanalysis) with the Niño-3 index and the SAM index. In both cases SLP variations are found along the path of the ACC, allowing for possible interactions between ocean dynamics and the atmospheric forcing pattern. The geostrophic flow induced by the anomalous pressure is expected to drive SST anomalies by advecting cold and warm air across the temperature front of the ACC.

The surface pressure pattern associated with SAM has an annular shape, but it is not exactly zonally symmetric: it extends to lower latitudes in the Pacific sector (Fig. 8). In that same region, the ACC streamlines bend toward the continent as the current flows through Drake Passage. As a result, the ACC intercepts a zone of strong pressure gradients, which will affect the heat fluxes in the ocean. In contrast, the ENSO teleconnection is more localized to the eastern Pacific sector. El Niño events are associated with a high pressure center (low pressure during La Niña).

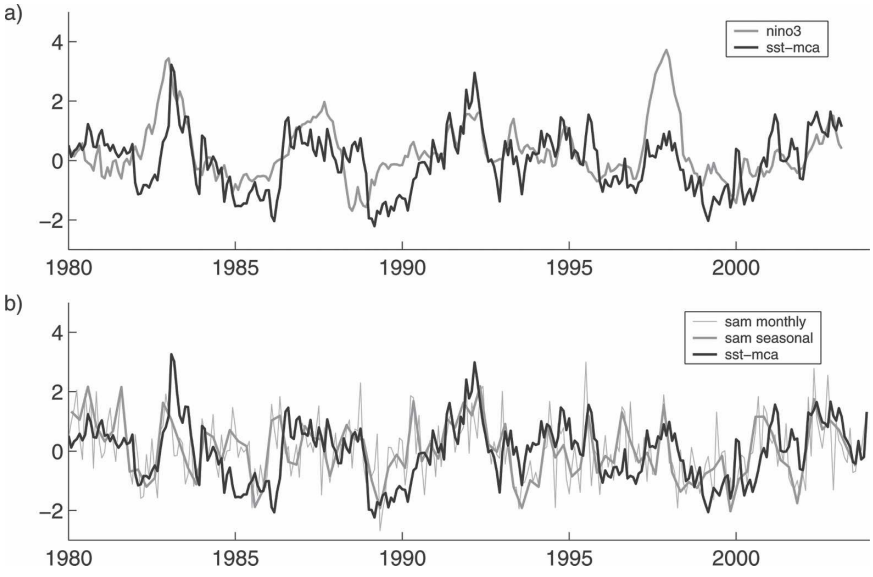

FIG. 7. Time series of SST-mca (black line): (a) Niño-3 (gray line) and (b) SAM index [monthly data (thin gray line) and seasonal averages (thick gray line)]. Each index is normalized.

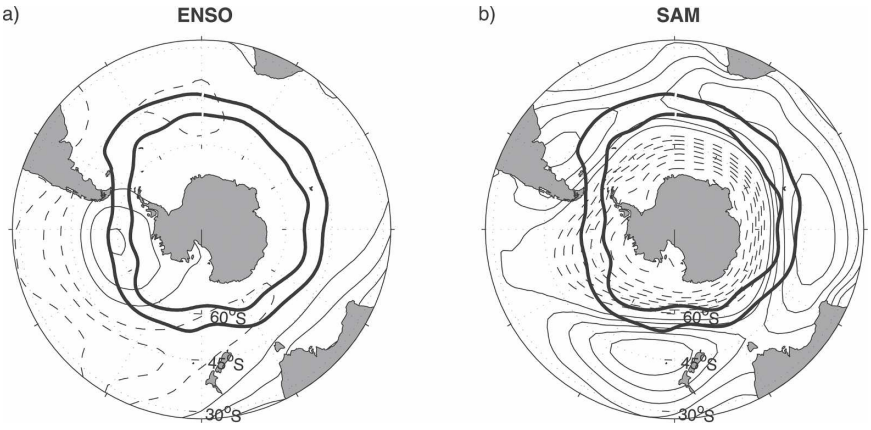

FIG. 8. Correlation of SLP with (a) Niño-3 and (b) SAM index; solid (dashed) contours indicate positive (negative) correlations. The contour interval is 0.1; the zero contour is not drawn. Thick black lines show the mean position of the ACC as defined in section 2. In the ACC band, both signals exhibit a strong pressure anomaly in the southeast Pacific.

b. SAM and ENSO heat flux patterns

Here, we analyze the spatial patterns associated with heat fluxes induced by ENSO and SAM, in order to illuminate their role in the generation of SST anomalies. This is done by regressing the heat fluxes onto the SAM index and Niño-3 index. The resulting spatial patterns are shown in Fig. 9. These patterns correspond to the heat fluxes occurring during an anomalous index with an amplitude of 1 standard deviation (1σ). The spatial pattern multiplied by the index time series gives the actual observed heat fluxes.

As evidenced in Fig. 9, the heat flux variability induced by ENSO occurs principally in the Pacific sector, which is consistent with the location of the ENSO-driven low-level circulation pattern (Fig. 8). In an El Niño year, anomalous meridional advection along the path of the ACC leads to surface warming in the central Pacific, and cooling in the western Pacific and downstream of Drake Passage. At the same time, Ekman advection in the ocean induces warming in the Pacific sector. The signs of the fluxes are reversed during a La Niña episode. Surface heat fluxes and Ekman heat fluxes interact constructively in the central Pacific; this region coincides with the location where SST variance is observed to be maximum.

SAM displays a similar pattern of surface heat fluxes, with a tripole structure in the Pacific sector. This is superimposed on a zonally symmetric signal associated with Ekman heat fluxes. The latter is efficient in driving cooling of the upper ocean in the ACC band during a positive phase of the annular mode. Once again, the two patterns of simultaneous variability enhance each other in the central Pacific.

c. SAM and ENSO impact on SST

We now assess the relative importance of the heat fluxes driven by ENSO and SAM, in explaining the observed SST. The heat fluxes regressed on ENSO and SAM are introduced in the flux model of section 3. We construct a matrix of the forcing: spatial patterns, seasonally varying, multiplied by the index time series (SAM index and Niño-3). Note that here the spatial patterns are calculated for each of the four seasons, to account for the fact that heat fluxes are different in the summer than in the winter (Fig. 9 shows the annual mean patterns).

Simulated SSTs are presented in Fig. 10. The simulation with both fields is simply the sum of the simulation with ENSO and the simulation with SAM, since the model is linear. The simulation with ENSO reproduces the strong events of 1982–83 and 1997–98. However, it seems as though most of the higher-frequency variability is induced by SAM. Both sources of external forcing are associated with SST variability in the Pacific basin.

We can test the relevance of the simulated field to the observations by comparing their first EOF. The correlation coefficients between the time series are 0.57 for the ENSO-only simulation, 0.63 for the SAM-only simulation, and 0.70 for the simulation with both fields. The best simulations are obtained with both SAM- and ENSO-induced heat fluxes, which suggests that they are both important in creating the observed SST variability.

In all three cases, the correlation is higher than that obtained for the simulation with the total heat fluxes (section 3c). This implies that the mode of variability

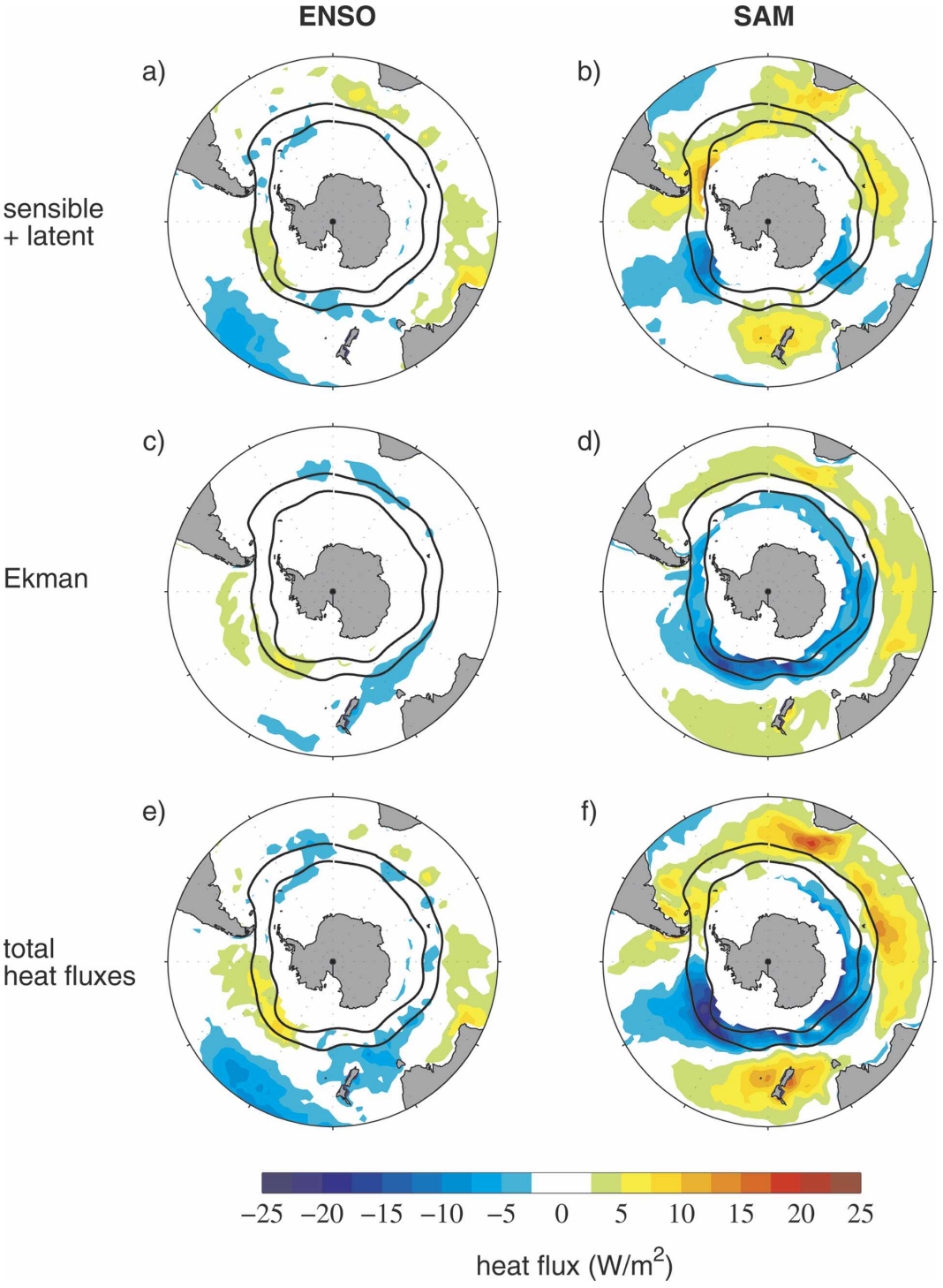

FIG. 9. Regression of monthly heat fluxes anomalies (W m^{-2}) onto (left) Niño-3 and (right) SAM index for (a), (b) the surface turbulent heat fluxes (sensible + latent); (c), (d) the Ekman heat fluxes; and (e), (f) the sum of the two components (surface + Ekman). Heat fluxes are defined as positive when into the ocean.

along the ACC that has a spatial pattern centered in the Pacific sector is better reproduced with ENSO- and/or SAM-induced forcing. It suggests that other components of the forcing reduce the quality of the simulation. These results support our hypothesis that SAM and ENSO are two drivers of SST variability along the ACC (section 4a) and that their effect is concentrated in the Pacific basin (Fig. 8).

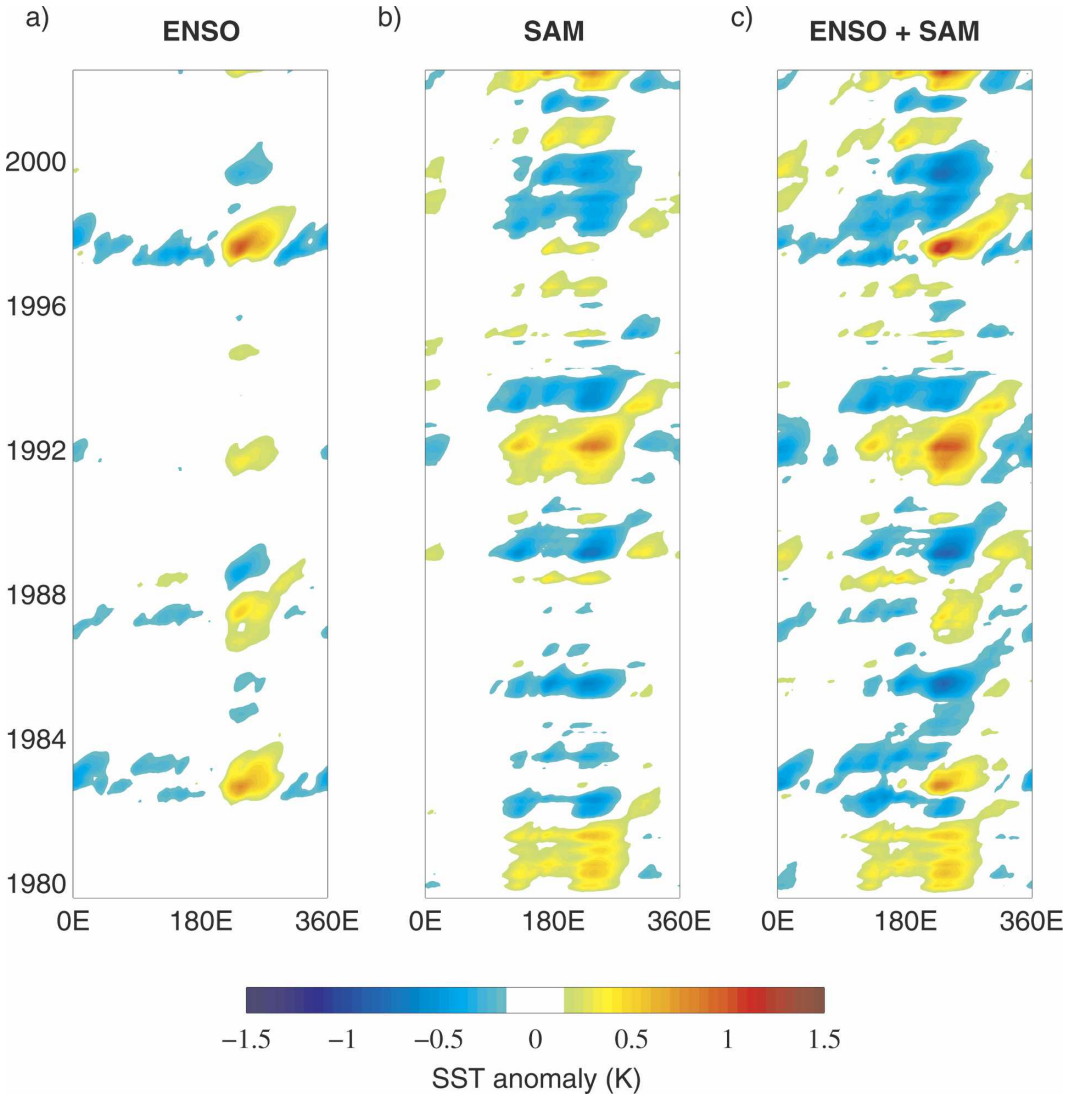

FIG. 10. Time–longitude diagrams showing the SST simulated from the heat fluxes regressed on (a) Niño-3, (b) SAM, and (c) Niño-3 + SAM.

5. Spectral response of SST to stochastic forcing

Having identified SAM and ENSO as the dominant sources of atmospheric forcing, we now relate their impact on SST to the advective resonance mechanism proposed by Saravanan and McWilliams (1998), which can be extended to periodic domains such as the ACC region (Weisse et al. 1999; Scott 2003). We begin by reviewing some important concepts of the mechanism; a more complete discussion is found in Weisse et al. (1999).

a. Resonant advection mechanism

The ocean's response to stochastic forcing, in the presence of a mean oceanic flow, depends on the advection speed and the time scale for the dissipation of SST anomalies. In the model of section 3, we introduced a damping term, α; that term did not include the dissipation of temperature anomalies via air–sea heat fluxes, which was already accounted for in the F_s' term of (4) (F_s' includes both the effects of atmospheric forcing and oceanic feedbacks). The total damping, including air–sea heat fluxes, will be represented by the symbol λ; it is equivalent to the λ_{eff} of (9) in Saravanan and McWilliams (1998).

The temperature equation in (4) can be rewritten (dropping the primes)

$$\frac{\partial}{\partial t} T + \overline{u} \frac{\partial}{\partial x} T = -\lambda T + F, \tag{5}$$

where F represents the surface and Ekman heat flux forcing, F'_{ek} and F'_s in (4); the factor $\rho c_p h$ is absorbed in the variables λ and F.

From (5) we can relate the SST spectrum (E_T) to the spectrum of the forcing (E_F):

$$E_T(\omega, k) = \frac{E_F(\omega, k)}{(\omega - k\bar{u})^2 + \lambda^2}, \quad (6)$$

where the $k\omega$ spectrum E_X is defined as $E_X = \langle \hat{X}\hat{X}^* \rangle$; $\bar{u}$ is the mean advective velocity, k is the spatial wavenumber, ω is the angular frequency, and brackets denote ensemble average.

If the forcing is a white noise, then $E_F = E_F(k)$; it does not depend on the frequency. In that case, (6) predicts a peak in the ocean $k\omega$ spectrum at the frequency $\omega = k\bar{u}$. If the forcing has a dominant wavenumber k_0, the peak is located at $\omega = k_0\bar{u}$, corresponding to an advective time scale of

$$T_{adv} = \frac{2\pi}{k_0\bar{u}}. \quad (7)$$

This time scale appears as the preferred period of oceanic variability, even though the atmospheric forcing is white. It corresponds to the Fourier mode for which the reversal of the polarity of the forcing (one-half of a period) takes the same time as the advection of SST anomalies between two poles of the sinusoidal forcing pattern (one-half of a wavelength); anomalies created under one pole thus get amplified under the next pole. This results in SST anomalies that are long lived, propagate at the speed of the ocean current and have a preferred time scale in the SST spectrum. All other frequencies (Fourier modes) interact destructively with the ocean.

In a periodic domain such as the Southern Ocean, the resonance mechanism would lead to an infinite SST response if there were no damping or friction; the original scenario of anomalies propagating in a bounded domain (Saravanan and McWilliams 1998) is a "finite resonance," since the SST response would remain finite even if the damping vanished.

In the ocean, $\bar{u}$ is rather small, typically a few centimeters per second, and k_0 is also small when large-scale forcing is considered. Thus, T_{adv} is large, which means that the oceanic variability induced by stochastic forcing has a low frequency, ranging from interannual to decadal variability.

b. Spectral response to ENSO and SAM

To relate SAM and ENSO forcing to the advective resonance mechanism, we have reconstructed the $k\omega$ forcing spectrum of SAM and ENSO, from the heat flux patterns shown in Fig. 9. To do so, we have written the forcing spectrum as a product $E_F(\omega, k) = E_F(\omega)E_F(k)$, in which $E_F(k)$ is simply obtained from a Fourier transform of the streamline-averaged pattern shown in Figs. 9e and 9f, and in which $E_F(\omega)$ is taken as a white noise (with amplitude determined from a linear regression). The latter procedure is justified from a study of the time series associated with the patterns in Figs. 9e and 9f, which have a decorrelation time scale of about a month (not shown).

The resulting spectra are presented in Fig. 11. In both spectra, most of the variability occurs at low wavenumbers; this reflects the spatial pattern of the total heat fluxes, for which $k = 1, 2$ are the dominant Fourier components. Both ENSO and SAM spectra show enhanced power at a time scale of about 10 yr for $k = 1$ and 5 yr for $k = 2$ (note that the spectra are continuous in ω but discrete in k), both being in agreement with (7). It appears that SAM and ENSO contribute equally to the SST variability.

The short dataset does not warrant a direct comparison with observed spectra but the results obtained in Fig. 10 are in qualitative agreement with the spatiotemporal characteristics of SST discussed in section 2c. Decadal variability at low wavenumbers also appears to characterize the SST simulated with ENSO and SAM heat fluxes (Fig. 10). In particular, a $k = 1$ feature is evident.

6. Ocean–atmosphere coupling

In agreement with the modeling results of Weisse et al. (1999) and Haarsma et al. (2000), the present analysis suggests that low-frequency SST variability in the ACC can arise from the resonant response of the ocean to stochastic atmospheric forcing. Such a mechanism does not require ocean–atmosphere coupled dynamics. The identification of ENSO and SAM as drivers of anomalous low-level circulation further supports this hypothesis; SAM exists independently of ocean–atmosphere coupling, and the ENSO signal in the Southern Ocean is not affected by local ocean dynamics.

Since ENSO and SAM are the main generators of temperature anomalies along the path of the ACC (section 4), we suggest that SST variability in the Southern Ocean results primarily from a passive response of the oceanic mixed layer to atmospheric forcing, ocean–atmosphere coupling playing a second-order role.

7. Summary and conclusions

The spatial and temporal distribution of SST anomalies in the ACC is studied using observations and conceptual models. Low-frequency variability in the ocean

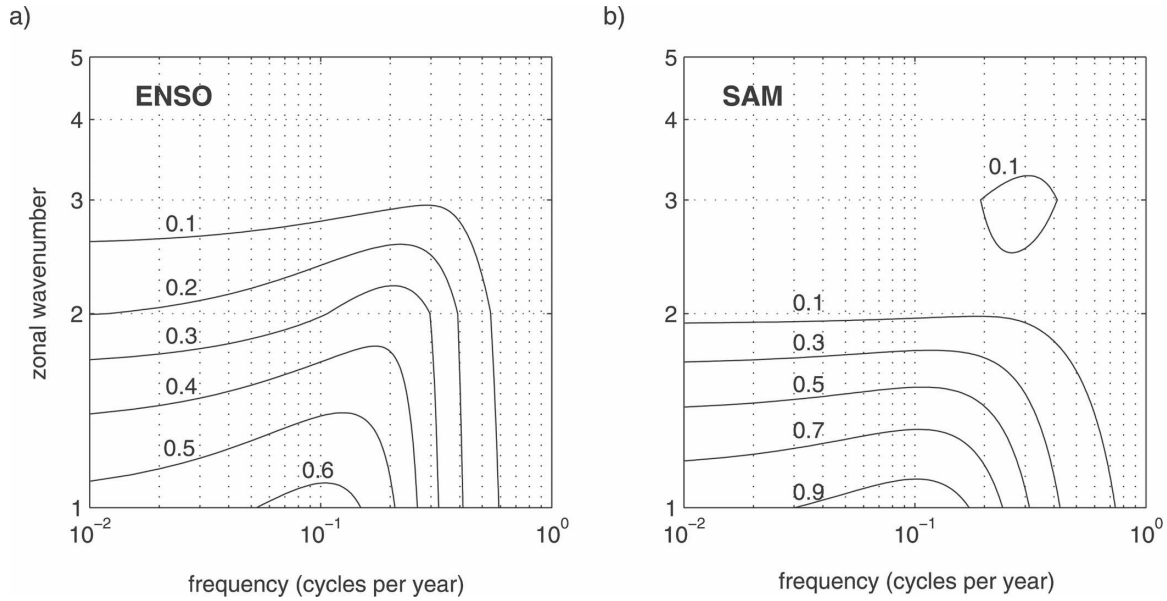

FIG. 11. Wavenumber–frequency spectrum for SST, as predicted from (4), assuming a white-noise forcing with the spatial pattern of (a) the heat fluxes regressed on ENSO, as shown in Fig. 9e, and (b) the heat fluxes regressed on SAM, as shown in Fig. 9f. Both spectra are normalized by the peak value of the SST spectrum in (b). The ocean response is expected to be at low wavenumbers, with a dominant period of 10 yr. Note that the spectrum is continuous in ω but discrete in k. The spectra were calculated with $\lambda \simeq (8 \text{ months})^{-1}$.

is related to fixed patterns of variability in SLP and anomalous surface forcing: turbulent heat fluxes (F_s) and Ekman advection (F_{ek}).

In summary, our main results are as follows.

(i) A simple model of SST including mean advection and driven by observed anomalous surface forcing ($F_s + F_{ek}$) provides a zero-order picture for SST anomalies along the ACC.
(ii) SAM and ENSO have a strong signature in F_s and F_{ek} over the eastern Pacific and act as generators of SST anomalies in that sector. The SST anomalies are subsequently advected by the mean current.
(iii) The damping of anomalies is large enough that they can be followed for only a couple of years. We found no indication of global propagation along the ACC.

The mechanisms investigated do not rely on ocean–atmosphere coupling. The generation, propagation, and damping of SST anomalies can be understood as a passive response of the ocean mixed layer to stochastic atmospheric forcing. Coupled ocean–atmosphere models might shed further light on the role of air–sea interactions in Southern Hemisphere climate variability, although our results suggest that the teleconnection with ENSO and the subtle asymmetry in the surface pattern of SAM need to be reproduced accurately in order to simulate the surface heat fluxes in the Pacific basin.

Examination of the heat fluxes along the ACC reveals that the air–sea interaction occurs mainly in the Pacific sector. In this region we also observe mode water formation. Subantarctic Mode Water (SAMW) results from deepening of the mixed layer in the winter; in the southeast Pacific it is exported as Antarctic Intermediate Water (Sloyan and Rintoul 2001) and plays an important role in the meridional overturning circulation. Rintoul and England (2002) have argued that SAMW variability is driven principally by Ekman transport, as opposed to local air–sea fluxes. The present study suggests that both mechanisms are important sources of oceanic variability.

Temperature variability also has implications for the interannual variability of CO_2 fluxes in the Southern Ocean. Heat fluxes affect the air–sea exchanges of gas by changing their solubility; because oceanic CO_2 equilibrates slowly with atmospheric concentrations, it exhibits variability at time scales longer than that of the forcing. Decadal variability in CO_2 fluxes is detected in data from the high-resolution global model of biogeochemical cycles of McKinley et al. (2003); it is likely to arise from stochastic atmospheric forcing, as in the case of SST, and could be investigated using the framework proposed in this study.

Acknowledgments. The NCEP–NCAR reanalysis data are provided by the IRI/LDEO Climate Data Library on their Web site (http://ingrid.ldeo.columbia.edu/). We thank Fabio d'Andrea for helpful discussions during the preparation of the manuscript and two anonymous reviewers for valuable comments and suggestions. This work was supported by the Office of Polar Programs of the National Science Foundation and the Office of Global Programs of the National Oceanic and Atmospheric Administration.

REFERENCES

Alexander, M. A., I. Bladé, M. Newman, J. R. Lanzante, N. C. Lau, and J. D. Scott, 2002: The atmospheric bridge: The influence of ENSO teleconnections on air–sea interaction over the global oceans. *J. Climate,* **15,** 2205–2231.

Bretherton, C. S., C. Smith, and J. M. Wallace, 1992: An intercomparison of methods for finding coupled patterns in climate data. *J. Climate,* **5,** 541–560.

Cai, W., and P. G. Baines, 2001: Forcing of the Antarctic circumpolar wave by El Niño–Southern Oscillation teleconnections. *J. Geophys. Res.,* **106,** 9019–9038.

Cane, M. A., S. E. Zebiak, and S. C. Dolan, 1986: Experimental forecasts of El-Niño. *Nature,* **321,** 827–832.

Czaja, A., P. van der Vaart, and J. Marshall, 2002: A diagnostic study of the role of remote forcing in tropical Atlantic variability. *J. Climate,* **15,** 3280–3290.

Frankignoul, C., 1985: Sea surface temperature anomalies, planetary waves, and air–sea feedback in the middle latitudes. *Rev. Geophys.,* **23,** 357–390.

Goodman, J. C., and J. Marshall, 1999: A model of decadal middle-latitude atmosphere–ocean coupled modes. *J. Climate,* **12,** 621–641.

——, and ——, 2003: The role of neutral singular vectors in midlatitude air–sea coupling. *J. Climate,* **16,** 88–102.

Haarsma, R. J., F. M. Selten, and J. D. Opsteegh, 2000: On the mechanisms of the Antarctic circumpolar wave. *J. Climate,* **13,** 1461–1480.

Hall, A., and M. Visbeck, 2002: Synchronous variability in the Southern Hemisphere atmosphere, sea ice, and ocean resulting from the annular mode. *J. Climate,* **15,** 3043–3057.

Hasselmann, K., 1976: Stochastic climate models. Part 1. Theory. *Tellus,* **28,** 473–485.

Kalnay, E., and Coauthors, 1996: The NCEP/NCAR 40-Year Reanalysis Project. *Bull. Amer. Meteor. Soc.,* **77,** 437–471.

Karoly, D. J., 1989: Southern Hemisphere circulation features associated with El Niño–Southern Oscillation events. *J. Climate,* **2,** 1239–1252.

Karsten, R. H., and J. Marshall, 2002: Constructing the residual circulation of the ACC from observations. *J. Phys. Oceanogr.,* **32,** 3315–3327.

Kushnir, Y., R. Seager, J. Miller, and J. C. H. Chiang, 2002: A simple coupled model of tropical Atlantic decadal climate variability. *Geophys. Res. Lett.,* **29,** 2133, doi:10.1029/2002GL015874.

Latif, M., and T. P. Barnett, 1994: Causes of decadal climate variability over the North Pacific and North America. *Science,* **266,** 634–637.

Levitus, S., and T. P. Boyer, 1994: *Temperature.* Vol. 4, *World Ocean Atlas 1994,* NOAA Atlas NEDSIS 4, 117 pp.

Liu, J., X. Yuan, D. Rind, and D. G. Martinson, 2002: Mechanism study of the ENSO and southern high latitude climate teleconnections. *Geophys. Res. Lett.,* **29,** 1679, doi:10.1029/2002GL015143.

Marshall, J., and Coauthors, 2001: North Atlantic climate variability: Phenomena, impacts and mechanisms. *Int. J. Climatol.,* **21,** 1863–1898.

McKinley, G. A., M. J. Follows, J. Marshall, and S.M. Fan, 2003: Interannual variability of air–sea O_2 fluxes and the determination of CO_2 sinks using atmospheric O_2/N_2. *Geophys. Res. Lett.,* **30,** 1101, doi:10.1029/2002GL016044.

Nakamura, H., and A. Shimpo, 2004: Seasonal variations in the Southern Hemisphere storm tracks and jet streams as revealed in a reanalysis dataset. *J. Climate,* **17,** 1828–1844.

Qiu, B., and F.-F. Jin, 1997: Antarctic circumpolar waves: An indication of ocean–atmosphere coupling in the extratropics. *Geophys. Res. Lett.,* **24,** 2585–2588.

Rintoul, S. R., and M. H. England, 2002: Ekman transport dominates local air–sea fluxes in driving variability of Subantarctic Mode Water. *J. Phys. Oceanogr.,* **32,** 1308–1321.

Saravanan, R., and J. C. McWilliams, 1998: Advective ocean–atmosphere interaction: An analytical stochastic model with implication for decadal variability. *J. Climate,* **11,** 165–188.

Scott, R. B., 2003: Predictability of SST in an idealized, one-dimensional, coupled atmosphere–ocean climate model with stochastic forcing and advection. *J. Climate,* **16,** 323–335.

Sloyan, B. M., and S. R. Rintoul, 2001: Circulation, renewal, and modification of Antarctic Mode and Intermediate Water. *J. Phys. Oceanogr.,* **31,** 1005–1030.

Sterl, A., 2004: On the (in)homogeneity of reanalysis products. *J. Climate,* **17,** 3866–3873.

Talley, L. D., 1999: Simple coupled midlatitude climate models. *J. Phys. Oceanogr.,* **29,** 2016–2037.

Thompson, D. W. J., and J. M. Wallace, 2000: Annular modes in the extratropical circulation. Part I: Month-to-month variability. *J. Climate,* **13,** 1000–1016.

Weisse, R., U. Mikolajewicz, A. Sterl, and S. S. Drijfhout, 1999: Stochastically forced variability in the Antarctic Circumpolar Current. *J. Geophys. Res.,* **104,** 11 049–11 064.

White, W. B., and R. G. Peterson, 1996: An Antarctic circumpolar wave in surface pressure, wind, temperature and sea ice extent. *Nature,* **380,** 699–702.

——, S.-C. Chen, and R. G. Peterson, 1998: The Antarctic circumpolar wave: A beta effect in ocean–atmosphere coupling over the Southern Ocean. *J. Phys. Oceanogr.,* **28,** 2345–2361.

Wunsch, C., 1999: The interpretation of short climate records, with comments on the North Atlantic and Southern Oscillations. *Bull. Amer. Meteor. Soc.,* **80,** 245–255.

Yuan, X., and D. G. Martinson, 2000: Antarctic sea ice extent variability and its global connectivity. *J. Climate,* **13,** 1697–1717.